University of Kent

Kent Academic Repository

Wang, Yongyue, Qian, Xiangchen, Wang, Lijuan and Yan, Yong (2023) *Measurement of Cross-sectional Velocity Distribution of Pneumatically Conveyed Particles in a Square-Shaped Pipe Through Gaussian Process Regression-Assisted Non-restrictive Electrostatic Sensing*. IEEE Transactions on Instrumentation & Measurement, 72 . ISSN 0018-9456.

Downloaded from

https://kar.kent.ac.uk/99441/ The University of Kent's Academic Repository KAR

The version of record is available from

https://doi.org/10.1109/TIM.2023.3238743

This document version

Author's Accepted Manuscript

DOI for this version

Licence for this version

UNSPECIFIED

Additional information

Versions of research works

Versions of Record

If this version is the version of record, it is the same as the published version available on the publisher's web site. Cite as the published version.

Author Accepted Manuscripts

If this document is identified as the Author Accepted Manuscript it is the version after peer review but before type setting, copy editing or publisher branding. Cite as Surname, Initial. (Year) 'Title of article'. To be published in ***Title of Journal*** , Volume and issue numbers [peer-reviewed accepted version]. Available at: DOI or URL (Accessed: date).

Enquiries

If you have questions about this document contact ResearchSupport@kent.ac.uk. Please include the URL of the record in KAR. If you believe that your, or a third party's rights have been compromised through this document please see our Take Down policy (available from https://www.kent.ac.uk/guides/kar-the-kent-academic-repository#policies).

Measurement of Cross-sectional Velocity Distribution of Pneumatically Conveyed Particles in a Square-Shaped Pipe Through Gaussian Process Regression-Assisted Non-restrictive Electrostatic Sensing

Yongyue Wang, Xiangchen Qian, *Senior Member, IEEE*, Lijuan Wang, *Senior Member, IEEE*, and Yong Yan, *Fellow, IEEE*

***Abstract*—Online continuous measurement of the cross-sectional velocity distribution of pneumatically conveyed solids in a square-shaped pipe is desirable in monitoring and optimizing circulating fluidized beds, coal-fired power plants and exhaust pipes. Due to the limitation of non-restrictive electrostatic sensors in spatial sensitivity, it is difficult to accurately measure the velocity of particles in large-diameter pipes. In this paper, a novel approach is presented for the measurement of cross-sectional particle velocity distribution in a square-shaped pipe using sensors and Gaussian process regression (GPR). The electrostatic sensor includes twelve pairs of strip-shaped electrodes. Experimental tests were conducted on a laboratory test rig to measure the cross-sectional particle velocities in a vertical square-shaped pipe under various experimental conditions. The GPR model is developed to infer the relationship between the input variables of velocities and the cross-sectional velocity distribution of particles in nine areas of the pipe cross-section and the performance of the built models was compared with other machine learning models. The relative error of velocities predicted under all the experimental conditions is within ±3%. When the training dataset is not comprehensive enough, the performance of the model is negatively affected, and the relative error range is –9% to +15%. With fewer measurement electrodes (input variables), the relative error of the predicted velocities in each area increases slightly, but remains within ±5%. Results obtained suggest that the electrostatic sensor in conjunction with the GPR model is a feasible approach to obtain the cross-sectional velocity distribution of pneumatically conveyed particles in a square-shaped pipe.**

***Index Terms*—two-phase flow, particle velocity, Gaussian process regression, square-shaped pipe, cross-sectional velocity distribution.**

I. INTRODUCTION

SQUARE-shaped pneumatic conveying pipes are commonly used in circulating fluidized beds and coal-fired power plants in certain countries, e.g., Poland and Germany [1], [2]. During the conveying processes, particles are irregularly distributed in the pipe cross-section due to the time-varying interphase forces, the variation of pipe direction, the properties of particles and the phase loading ratio. Therefore, cross-sectional velocity measurement of particles in gas–solid two-phase flows in square-shaped pipes is of great significance to understanding the dynamic behaviors of particles, obtaining a more accurate cross-sectional average particle velocity and the determination of the mass flow rate of solids. However, there is little research on the cross-sectional characterization of gas–solid two-phase flows in square-shaped pipes.

Due to the non-circle center symmetry and the existence of four right angles on the pipe wall, particle distribution in a square-shaped pipe is more complex than that in a circular-shaped pipe [2]. The radiometric, optical and microwave sensors can be used to measure the cross-sectional velocity distribution of particles in both circle and square pipes [3], [4]. An averaged particle velocity can be calculated based on the velocity distribution obtained by scanning the measurement point with a laser doppler velocimetry (LDV) system [5], [6]. However, the performance of this method is significantly influenced by the variation of flow status as the measurement takes a long time to complete. Dinardo *et al.* [6] used a laser Doppler anemometer (LDA) to measure the punctual velocities in the cross-section of a square-shaped pipe. They provided an empirical formula for evaluating the mean flow rate at a fixed location (approximately 0.78 of the transverse dimension on the main axis of the pipe section) in the pipe cross-section. However, the reliable determination of the averaged particle velocity in the pipeline in real-time requires synchronous measurements at several specific points. The methods mentioned above are unsuitable for industrial applications due to the high cost and susceptibility to interference from harsh industrial environments. Therefore, the limitations of conventional measurement methods need to be addressed

Manuscript received XXX; revised XXX; accepted XXX. Date of publication XXX; date of current version XXX. This work was supported by the National Natural Science Foundation of China under Grant 62273143. The Associate Editor coordinating the review process was XXX. (*Corresponding author: Xiangchen Qian.*)

Yongyue Wang and Xiangchen Qian are with the School of Control and Computer Engineering, North China Electric Power University, Beijing 102206, China (e-mail: y.wang@ncepu.edu.cn; xqian@ncepu.edu.cn).

Lijuan Wang and Yong Yan are with the School of Engineering, University of Kent, Canterbury, Kent, CT2 7NT, U.K. (e-mail: l.wang@kent.ac.uk; y.yan@kent.ac.uk).

Digital /ect Identifier XXXXXX

urgently.

Compared with the sensors mentioned in the above methods, electrostatic sensors have the advantages of simple structure, cost-effectiveness and suitability for a wide range of installation conditions [7]. Electrostatic sensors are based on the principle of electrostatic induction. Particularly, non-restrictive electrostatic sensors are more suitable for industrial applications because they exhibit a significant advantage in their non-restrictiveness to the movement of particles in a pipe [2]. But due to the fast weakening sensitivity with the increasing distance from the sensing electrode to moving particles, the use of non-restrictive electrostatic sensors demonstrates uncertain accuracy in the measurement of cross-sectional averaged velocity in large pipes under different flow conditions [7].

In recent years, soft computing techniques have been widely applied to facilitate the characterization of multiphase flows by establishing the relationship with the variables that can be measured directly [8]. For example, convolutional neural networks were developed for pattern identification of multiphase flows [9], [10], [11]. Artificial neural network (ANN) and support vector machine (SVM) were trained with experimental data to measure the mass flow rate and the fraction of individual phases in gas–solid or gas–liquid two-phase flows [12], [13], [14], [15], [16]. There is also research combining electrical capacitance tomography (ECT) techniques with deep-learning algorithms to visualize the dynamics of gas–liquid two-phase flow [17], [18]. The electrostatic sensor in conjunction with the trained models can also provide a simple, practical solution to the long-standing industrial measurement problem. Yan *et al*. [19] used a ring-shaped electrostatic sensor and principal component analysis preceded neural networks to measure the velocity and mass flow rate of pneumatically conveyed particles. Abbas *et al.* [20] introduced a technique for the mass flow rate measurement of pneumatically conveyed particles based on multimodal sensing and machine learning modeling. While the study applies soft computing techniques to cross-sectional velocity distribution measurement of particles in gas–solid two-phase flows is rare. However, with its wide application and superior performance in multiphase flow measurement, soft computing provides a new idea for the measurement of cross-sectional particle velocity distribution. Gaussian process regression (GPR) has been gradually recognized as a useful soft sensor modeling method over the past few years due to its excellent performance [21], [22]. Compared with common machine learning algorithms, including SVM, ANN and regression trees, GPR has good adaptability and strong generalization ability to deal with complex problems such as high dimensions, small samples and nonlinearity.

In order to improve the measurement performance of non-restrictive electrostatic sensors, this paper presents a novel approach incorporating electrostatic sensing with GPR modeling for the measurement of the cross-sectional velocity distribution of pneumatically conveyed particles in a square-shaped pipe. In this study, the particle velocities measured by twelve pairs of non-restrictive electrodes and the air velocity are used as the input variables of the model, while the output variables of the model are particle velocities in different areas of the pipe cross-section. Evaluation tests were undertaken to verify the performance of the proposed measurement approach. The concept along with preliminary results was initially reported at the 2022 IEEE International Instrumentation and Measurement Technology Conference [23]. This extended paper provides more experiments and analyses including a comparison of GPR's prediction results with other machine learning models, system design and explorations of improvement of the measurement approach.

II. METHODOLOGY

A. Overall Measurement Strategy

The overall strategy for the measurement of the cross-sectional velocity distribution of particles in a square-shaped pipe is shown in Fig. 1. The non-restrictive electrostatic sensor consisting of twelve pairs of strip-shaped electrodes is used to measure the velocity of particles moving through each electrode pair. A pair of identical parallel electrodes are used to determine particle velocity using a cross-correlation algorithm [7]. The air velocity is obtained with a measuring device suitable for the flow conditions. Then the particle velocities and the air velocity are considered as input variables to the model. In order to reduce the dimensionality of the datasets and increase interpretability, principal component analysis (PCA) is applied to the input variables. The vectors (i.e. principal components) from PCA are fed into the GPR model. Then the cross-sectional velocity distribution of particles in a square-shaped pipe is obtained by the GPR model.

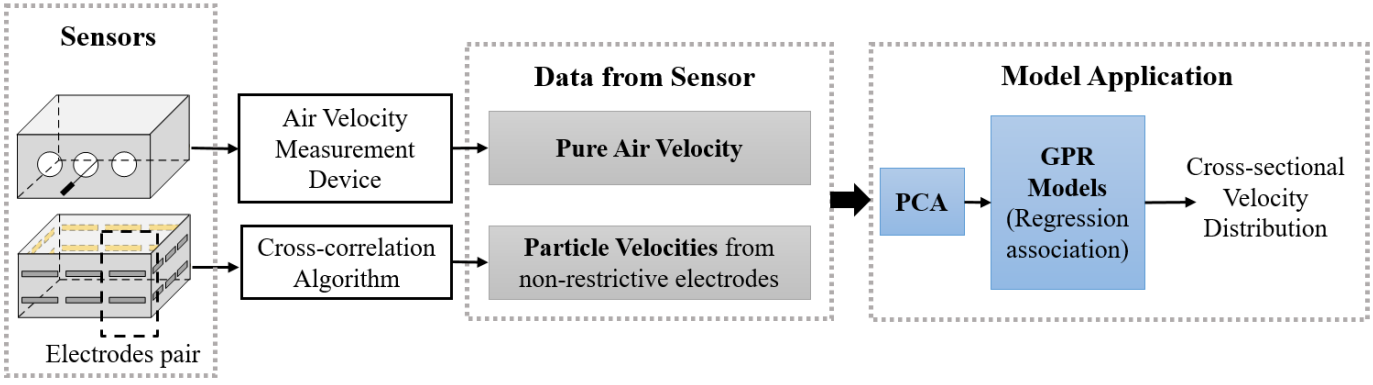

Fig. 1. Measurement strategy.

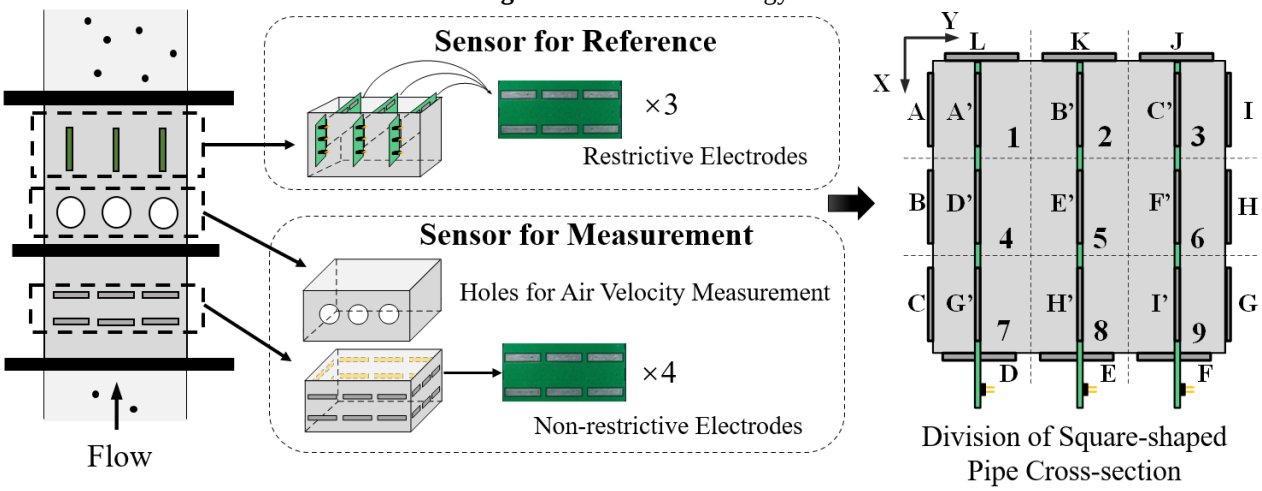

Fig. 2. Design of the sensor.

B. Structure of electrostatic sensors

The structure of the sensor used in this study is shown in Fig. 2. The holes on the pipe wall are used to insert a device for measuring the velocity of pure air. Non-restrictive sensors are used as measurement sensors for measuring the particle velocities to enter into the model as the input variables along with the air velocity. The restrictive electrostatic sensor is only employed in the model training process to provide the particle velocity in each area of the pipe cross-section as a reference. The reference velocities are used as the output variables of the model in the model training process. The restrictive electrostatic sensors can be removed when the reference value of particle velocity in each area of the pipe cross-section is obtained. The relationship between the velocities measured by the non-restrictive and restrictive sensors is established by GPR models. Then the real-time measurement of the particle velocity can be realized by the measurement sensor and the GPR model.

The non-restrictive electrostatic sensor consists of twelve pairs of strip-shaped electrodes (three pairs on each inner surface of the pipe). Two identical parallel electrodes, one being positioned downstream of the other, are used to determine particle velocity using a cross-correlation algorithm. The particle velocity can be derived from

$$v = \frac{L}{\tau} \tag{1}$$

where L is the center-to-center spacing between the upstream and downstream electrodes. The transit time required for the particles to move from the upstream electrode to the downstream electrode is represented by τ. In order to simultaneously obtain the reference velocities of particles in different areas of the pipe cross-section, the restrictive electrostatic sensor, including nine pairs of electrodes with the same dimensions as the non-restrictive electrodes, is installed downstream from the holes. The distance between the non-restrictive electrostatic sensor and the restrictive electrostatic sensor is 16 cm which is enough to avoid the turbulence caused by the restrictive electrostatic sensor.

In this study, the pipe cross-section with a side length of 54 mm is equally divided into nine sub-areas (index by A1 to A9) and each restrictive electrode is placed in the area center, as shown in Fig. 3. Therefore, the reference particle velocities of each area of the square-shaped pipe can be obtained by nine pairs of electrodes, respectively. Then the reference particle velocities of each area in the pipe cross-section are used as the output variables in the model training process.

C. Principal Component Analysis

The input variables for GPR model training include twelve particle velocities (namely v_A to v_L) obtained from twelve pairs of non-restrictive electrodes and the air velocity (v). PCA is used to remove the redundancy information and reduce the dimensionality of the predictor space, which can help prevent overfitting in the model training process. PCA is used to linearly transform the predictive factors, remove redundant dimensions, and generate a group of new variables called principal components. Firstly, the potential input variables are normalized as a matrix $W_{m\times n}$ and the covariance matrix C is calculated from:

$$C = \frac{1}{m} W W^T \tag{2}$$

where m is the dimension of W, which composes of the particle velocities obtained from the non-restrictive electrodes and the air velocity, and W^T is its transposed matrix. Then the eigenvalues λ and eigenvectors α of the matrix C can be determined from:

$$C\alpha = \lambda\alpha \tag{3}$$

The eigenvalues and corresponding eigenvectors are sorted by $\lambda_1 \geq \lambda_2 \geq \cdots \geq \lambda_n$. The eigenvalues are arranged into a matrix from top to bottom according to the corresponding eigenvectors, and the first k rows are taken to form a matrix M,

$$P = MW \tag{4}$$

where $P = \{p_1, p_2 \cdots p_k\}$ is the set of principal components, k is the reduced dimension. The resulting principal components are uncorrelated and arranged in descending order according to

their significance contributing to the overall data variation. The contribution of P is defined as

$$\alpha_k = \frac{\sum_{i=1}^{k}\lambda_i}{\sum_{i=1}^{n}\lambda_k}(k \le n) \tag{5}$$

In this study, PCA keeps enough components to explain 95% variance.

D. Gaussian Process Regression

The difference between the GPR algorithm and general machine learning algorithms such as regression trees, SVM and ANN is its flexible non-parametric nature and computational simplicity [22], [24]. The GPR can obtain the whole distribution of predicted values and give confidence intervals in terms of probability [25].

GPR is a non-parametric kernel-based probabilistic model that uses Gaussian process (GP) priors to perform regression analysis on data. Given a training dataset $D = \{(x_n, y_n)\}$, where x_n represents the input of data point n and y_n is the associated output, $X = [x_1, x_2, \dots, x_n]$ is the input matrix and $y_i \in \mathrm{R}$ is the corresponding output, y is output vector. In this study, the input is the principal components diverted from PCA and the output is the corresponding particle velocities in different areas of the pipe cross-section. Assume that the mapping between the training set and the output is $f(X)$, and $f(x_1), \dots f(x_n)$ form a set of random variables with a joint Gaussian distribution. The properties of $f(x)$ are determined by its mean function $\mu(x)$ and the covariance function $k(x, x')$. The random process $f(x)$ is a Gaussian process which can be expressed as:

$$f(x) \sim GP(\mu(x), k(x, x')) \tag{6}$$

where $\mu(x)=E(f(x))$. Usually, the mean function $\mu(x)$ is taken to be zero. A standard GPR model can be obtained by

$$y = f(X) + \varepsilon \tag{7}$$

where $\varepsilon \sim N(0, \sigma^2)$ is the homoscedastic Gaussian noise, σ^2 is the variance of noise. Then the prior distribution of the observation target values y can be obtained as follows:

$$y \sim N(0, K(X, X) + \sigma^2 I) \tag{8}$$

where

$$K(X,X) = \begin{pmatrix} k(x_1,x_1) & k(x_1,x_2) & \cdots & k(x_1,x_n) \\ k(x_2,x_1) & k(x_2,x_2) & \cdots & k(x_2,x_n) \\ \vdots & \vdots & \vdots & \vdots \\ k(x_n,x_1) & k(x_n,x_2) & \cdots & k(x_n,x_n) \end{pmatrix} \tag{9}$$

is a symmetric positive definite covariance matrix, $k(x_i, x_j)$ is the kernel function and I is a n-dimensional unit matrix.

The joint probability distribution of the training datasets and test datasets still meets a Gaussian distribution. GPR aims to forecast $f*$ by the given input $X*$ of test points. The joint distribution of the training output y and the test output values $f*$ under the prior is

$$\begin{bmatrix} y \\ f* \end{bmatrix} \sim N\left(0, \begin{bmatrix} K(X,X)+\sigma^2 I & K(X,X*) \\ K(X*,X) & K(X*,X*) \end{bmatrix}\right) \tag{10}$$

If there are n training points and $n*$ test points, then $K(X, X*)$ denotes the $n \times n*$ matrix of covariance evaluated at all pairs of training and test points, $K(X, X)$ is the $n \times n$ covariance matrix of inputs of training dataset D, and $K(X*, X*)$ is the covariance of the test points. The posterior distribution of $f*$ is given by:

$$f* \mid X, y, X* \sim N(\bar{f}*, \mathrm{cov}(f*)) \tag{11}$$

where

$$\bar{f}* = K(X*, X)[K(X, X) + \sigma^2 I]^{-1} y, \tag{12}$$

$$\mathrm{cov}(f*) = K(X*, X*) - K(X*, X)[K(X, X) + \sigma^2 I]^{-1} K(X, X*) \tag{13}$$

are the predicted mean and variance of the output, respectively. Therefore, the GPR model can predict the output of the test dataset based on the mean function, covariance function and the training samples, which can give the expected prediction results (mean value) and the uncertainty of measurement information (variance) of the output.

Due to the complex dynamic characteristics of gas–solid two-phase flows in a pipeline, it is difficult to estimate the properties of the underlying function for the problem under study. For the same reason, the modelling process is not based on prior knowledge. Instead, the cross-validation method is used to select the appropriate kernel functions. Four possibly applicable kernel functions, namely the exponential kernel (EK), squared exponential kernel (SEK), Matern 5/2 (M52K) and rational quadratic kernel (RQK) as shown below, are tested to select the one that produces a better prediction performance (Section IV-B).

$$k_{EK}(x_i, x_j) = \sigma_f^2 \exp(-\frac{r}{2\sigma_l^2}) \tag{14}$$

$$k_{SEK}(x_i, x_j) = \sigma_f^2 \exp(-\frac{r^2}{2\sigma_l^2}) \tag{15}$$

$$k_{M52K}(x_i, x_j) = \sigma_f^2 (1 + \frac{\sqrt{5}r}{\sigma_l} + \frac{5r^3}{3\sigma_l^2}) \exp(-\frac{\sqrt{5}r}{\sigma_l}) \tag{16}$$

$$k_{RQK}(x_i, x_j) = \sigma_f^2 (1 + \frac{r^2}{2\alpha\sigma_l^2})^{-\alpha} \tag{17}$$

where α is a positive-valued scale-mixture parameter, σ_l is the characteristic length scale, σ_f is the height scale and

$$r = \sqrt{(x_i - x_j)^T (x_i - x_j)} \tag{18}$$

is the Euclidean distance between x_i and x_j.

E. Bayesian hyperparameter optimization

The hyperparameters of the GPR model can be adjusted to obtain optimal performance. Bayesian optimization (BayesOpt) is a method for performing global optimization of an unknown "black box" objective function. The flowchart of the BayesOpt is given in Fig. 3. Starting from the prior function (GP), at each iteration, the posterior distribution is calculated by taking the previous evaluations of the objective function as the observed values in a Bayesian nonlinear regression. The goal of BayesOpt is to find an input that maximizes the acquisition function and then submit it to the function evaluation. The model can be updated when a new result is obtained, the acquisition function can be recomputed and a new input is chosen for evaluation, which means one iteration of the BayesOpt loop is completed. The acquisition functions are "expected improvement", "probability of improvement", etc.

[26]. In this study, the optimization of hyperparameters are implemented with the "Regression Learner App" (RLA) in MATLAB 2021b. The option of acquisition function is the "expected improvement per second plus". The RLA tries different combinations of hyperparameter values by using an optimization scheme that seeks to minimize the MSE of the model. The algorithm stops after reaching any of the following criteria, i.e. a fixed number of iterations (default is 30), a fixed time (default is no time limit), or stop criterion provided by people. In this study, the algorithm terminates after 30 iterations, because no obvious improvement is observed when the number of iterations is beyond 30.

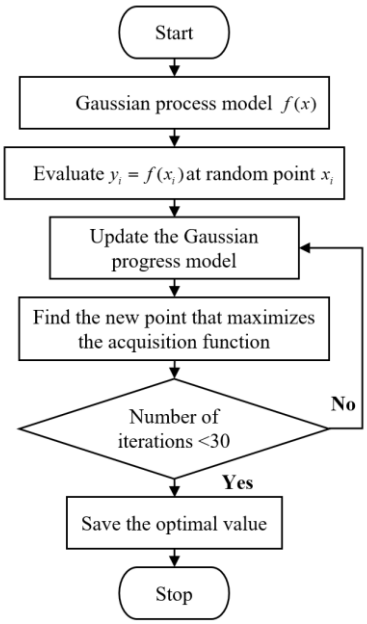

Fig. 3. Flowchart of Bayesian optimization algorithm.

F. Evaluation index

In order to compare the training error of the models, three common indexes, namely root mean square error (RMSE) and determination coefficient (R^2), are calculated based on the reference particle velocities and the predicted particle velocities from the model. By comparing RMSE, the performance of the trained models can be comprehensively evaluated. The coefficient of determination R^2 is an indicator to evaluate the degree of fitting of the model. The closer R^2 is to 1, the better the fit. The equation of each evaluation index is as follows:

$$RMSE = \sqrt{\frac{1}{m}\sum_{i=1}^{m}(y_i - \hat{y}_i)^2} \tag{17}$$

$$R^2 = 1 - \frac{\sum_i (y_i - \hat{y}_i)^2}{\sum_i (y_i - \bar{y}_i)^2} \tag{18}$$

where m is the number of test data, y_i is the reference value of the i-th test, $\hat{y}_i$ is the predicted value of the i-th test, $\bar{y}_i$ is the average of the reference values for m sets of test data. In addition, the error of the measurement approach in this study is evaluated using the relative error.

III. IMPLEMENTATION AND EVALUATION OF MEASUREMENT SYSTEM

Fig. 4 shows the implementation of the sensor system. The sensor is covered by a grounded shielding case to eliminate external electromagnetic interference [2]. All the stripe-shaped copper electrodes have the same dimension with a length of 15 mm and a width of 3 mm, and the center-to-center spacing between two adjacent electrodes (L) is 15 mm [2]. The side length of the pipe is 54 mm. Each electrode embedded in the sensor was connected by a shielded wire to a signal conditioning circuit, by which the electric current signals from the electrodes were converted into voltage signals and then amplified and filtered [27]. The signal conditioning circuits were installed in an earthed metallic box to minimize external electromagnetic interference. The conditioned signals were sampled by a data acquisition card (DAQ) for the calculation of particle velocity. As shown in Fig. 5, experimental tests were carried out on a laboratory-scale test rig consisting of a feeding system, a powder recovery, a negative pressure system and the electrostatic sensors. The particles (plain flour) used in this study are within the range of 98 to 124 μm. Solid particles were fed into the pipe using a double screw feeder and pneumatically conveyed to a solids recycling tank using a negative pressure system. The mass flow rate of particles and the conveying velocity can be changed by adjusting the double screw feeder and the negative pressure device, respectively. As shown in Fig. 5, the sensors were installed on a vertical pipe about 1200 mm away from the upstream elbow. The non-restrictive and the restrictive electrostatic sensors were used to measure the particle velocities simultaneously.

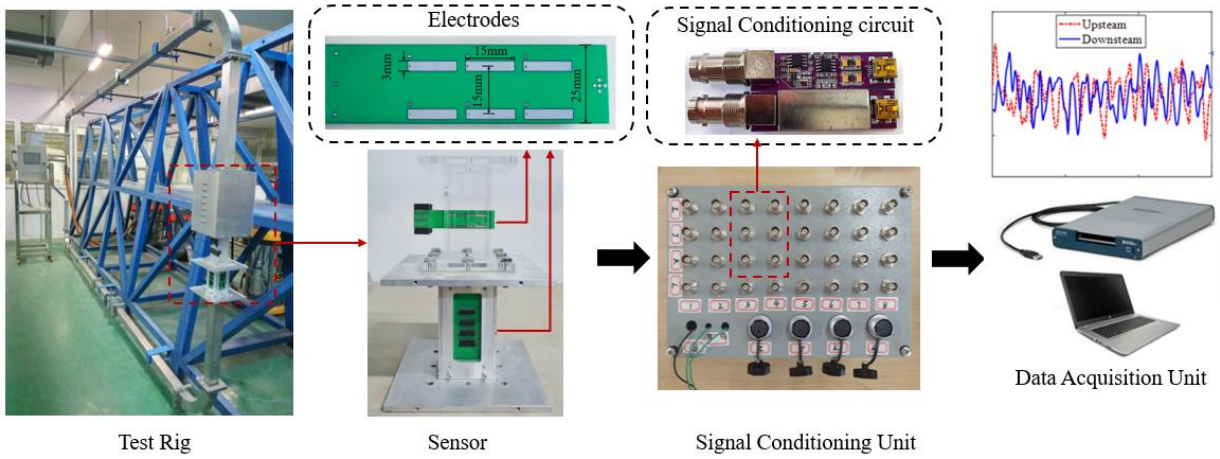

Fig. 4. Implementation of the measurement system

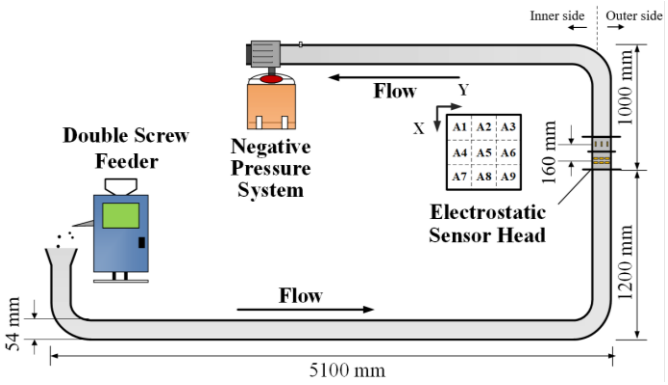

Fig. 5. Layout of the test rig.

TABLE I
EXPERIMENTAL CONDITIONS

Mass Flow (kg/h)	Air velocity (m/s)			
	V1=19	V2=23	V3=27	V4=31
M1=2	V1M1	V2M1	V3M1	V4M1
M2=4	V1M2	V2M2	V3M2	V4M2
M3=6	V1M3	V2M3	V3M3	V4M3
M4=8	V1M4	V2M4	V3M4	V4M4

The data used in this study were obtained from 16 experimental conditions (V1M1 to V4M4) as outlined in Table I. The air velocity and mass flow of particles were adjusted from 19 m/s to 31 m/s and 2 kg/h to 8 kg/h, respectively. The air velocity of each experimental condition was measured by a hot-wire anemometer (Model MP210, KIMO, France) before each particle flow test. The sampling frequency of the sensor measurement signal was 25 kHz. Several sets of replicate experiments were carried out for at least 60 s (signals were continuously collected). Each velocity value was calculated using 2000 sampled signals. During the experiments, the ambient temperature (around 26°C), relative humidity (around 69%) and particle characteristics (i.e. size, type, moisture content, etc.) were all controlled and almost constant. A total of 4496 groups of datasets were obtained for model training and testing. Each group of the dataset contains 12 columns of particle velocities measured by non-restrictive electrostatic electrode pairs, one column of air velocities and nine columns of particle reference velocities measured by restrictive electrostatic electrode pairs. All the modeling and data analysis work were carried out on a computer with Intel Core i7 3.60 GHz and 16 GB of RAM.

Usually, the velocity measured by each electrode pair of the non-restrictive sensor is regarded as the mean particle velocity in the pipeline under the steady state of the flow [28]. Fig. 6. shows the comparison of the average particle velocity of the pipeline section obtained by the non-restrictive electrostatic sensor (the mean value of v_A to v_L) and the restrictive electrostatic sensor (the mean value of reference particle velocities in nine areas). As shown in Fig. 6, the mean value of particles measured by the non-restrictive electrodes was more than 3 m/s slower than the mean value of the reference particle velocity (measured by the restrictive electrodes) under different experimental conditions, which shows that the particles are not uniformly distributed in the cross-section of the pipe during transportation. Due to the influence of the electrode sensitivity area, less error between the particle velocity measured by an restrictive electrode and the true value of the particle velocity compared to a non-restrictive electrode [29]. As shown in Fig. 6, in general, the velocity difference increases slightly with air acceleration, but shows a non-linear relationship. Therefore, the GPR models were used to extend the measurement performance of non-restrictive electrostatic sensors, which is of great significance for obtaining a more accurate average particle velocity and understanding the distribution of the particles in the pipeline section.

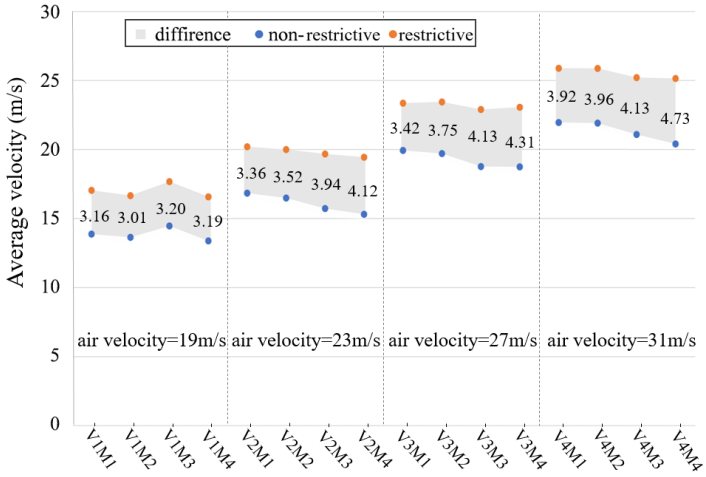

Fig. 6. Difference of measured particle velocities between non-restrictive and restrictive sensors.

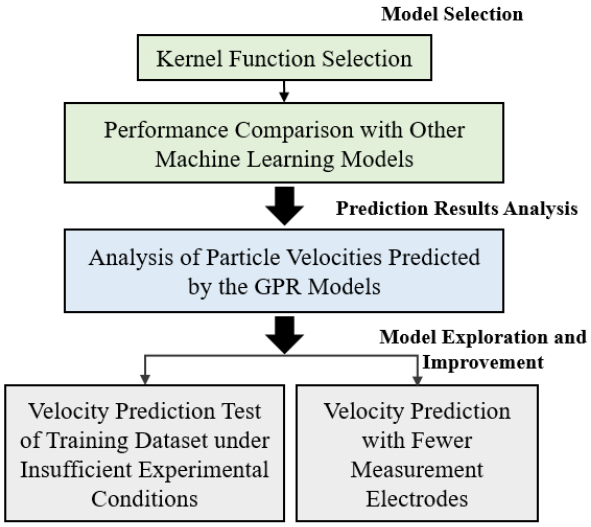

Fig. 7. Process of modeling and analysis

IV. MODELING AND ANALYSIS

A. Process of modeling and analysis

The GPR model selection experiments (subsections B and C), analysis of model prediction results (subsection D) and model improvement experiment (subsections E and F) are presented

successively in this section (as shown in Fig. 7). The experiments for model selection determine the GPR kernel function and make comparison with other commonly used machine learning algorithms, i.e., regression trees (RT), support vector machine (SVM), random forest (RF) and artificial neural network (ANN). Based on the predicted particle velocities in local areas of the pipe cross-section, the distribution of particle velocities in the pipe cross-section and the relative error of the predicted values in each area were analyzed. Subsections E and F present the test of training datasets with insufficient experimental conditions and velocity prediction with fewer measurement electrodes, respectively. By comparing the results of these two parts with those in Section D, some guidance on data acquisition, sensor layout design and input variables selection for the practical application of this method are concluded.

B. Kernel Function Selection

The optimal kernel function can be considered by comparing the prediction effect of models based on different kernel functions. In order to evaluate the effects of different kernel functions (EK, SEK, M52K and RQK) on the model performance, four GPR models with different kernel functions were developed based on the same training dataset, respectively. The RMSE results of predicted velocities from four GPR models in areas A1 to A9 are shown in Fig. 8. As can be seen from Fig. 8, the GPR model with the EK kernel function has the lowest RMSE than other models in all areas except for A1 and A6. The difference in RMSE between the GPR model with the EK kernel function and the best-performed model is less than 0.5%. Therefore, the exponential kernel function is selected to measure the cross-sectional velocity distribution under experimental conditions.

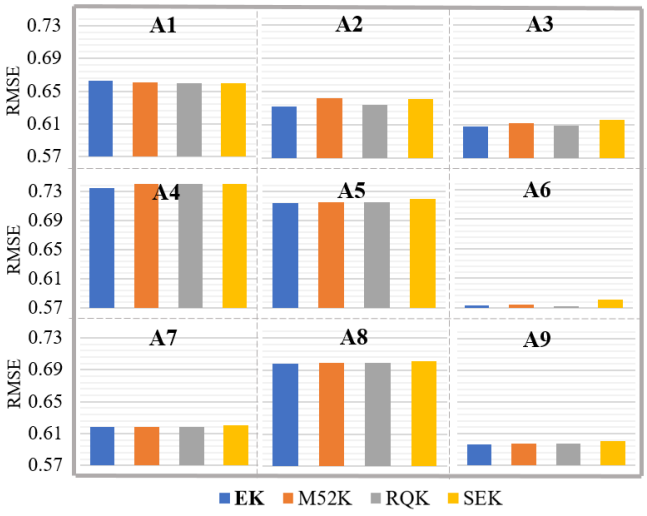

Fig. 8. Comparison of RMSE for four GPR models with different kernel functions.

C. Performance Comparison with other machine learning models

In order to validate the performance of the proposed models, a comparison analysis was conducted with RT, SVM, RF and ANN. In the model training process, the principal component vectors obtained from PCA were taken as the input of all the models. The reference particle velocity of each area was regarded as the output variable of the models. The models were set to the default values and the 5-fold cross-validation was applied in the model training process to evaluate the prediction performance of the models, which can also avoid overfitting.

In the model comparison process, this study focuses on the combined performance of the models in different areas of the pipeline, especially the performance of the models in the central region of the pipeline. The prediction results show that, in each area, GPR exhibits optimal performance compared to other models. The results for the central area of the pipeline (A5) are shown as an example in Table II, in which the RMSE, the time taken for prediction and R^2 of the 5 models are listed. As can be seen from Table II, RT requires the least prediction time because fast in fitting and prediction progress and occupies less memory, but has the lowest R^2, which means that its fitting effect is the worst. RF is improved based on RT and sampled with the training dataset by the bootstrap method. SVM has a balanced performance. ANN models have good prediction accuracy. However, they are not easily interpreted and the flexibility of the models increases with the size and number of fully connected layers in the neural network. In this study, the ANN models used for comparison have two fully connected layers because it was found through experiments that the single-layer neural network did not perform well in particle velocity prediction in some areas, the three-layer neural network experienced overfitting and performed poorly on the test set. Fig.9 shows the mean value of the evaluation index of 9 areas. GPR models show the minimum prediction error (the minimum value of RMSE) and the best fitting effect (the maximum value of R^2), although its prediction speed is the slowest (about 12000 observations per second). The results demonstrate that the prediction performance of the GPR model is better than that of the other five models, and the time consumption can also meet the requirement for the measurement of the particle velocity in industrial applications.

TABLE II
PREDICTED ERRORS AND CALCULATION TIME OF DIFFERENT MODELS IN A5

Model	RMSE	R^2	Prediction speed (obs/s)
GPR	0.715	0.96	9900
RT	0.841	0.94	68000
SVM	0.810	0.94	26000
RF	0.765	0.95	22000
ANN	0.819	0.94	45000

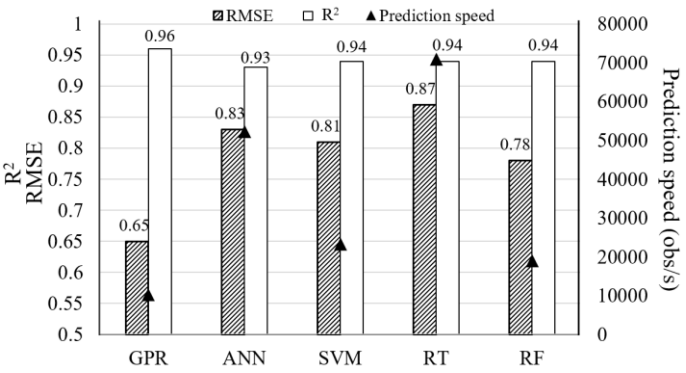

Fig. 9. Mean values of evaluation index of different models in 9 areas.

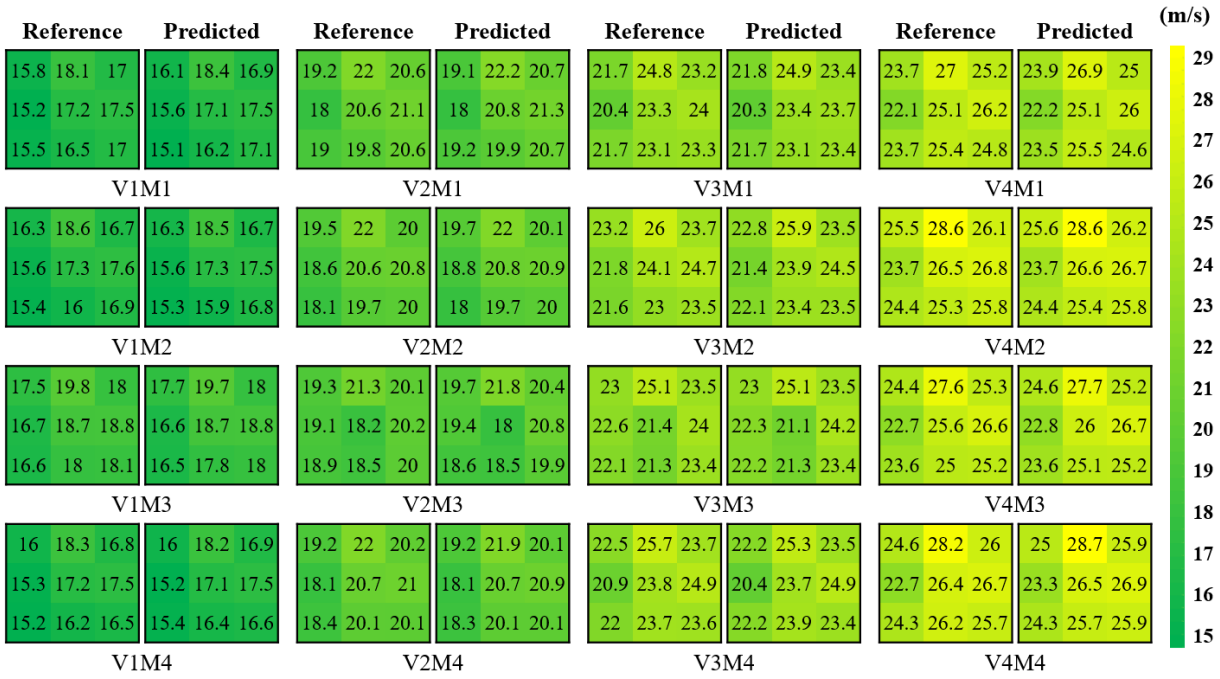

Fig. 10. Comparison of the predicted and reference velocities of the particle under 16 experimental conditions.

D. Analysis of Particle Velocities Predicted by the GPR Models

The relationship between the principal component vectors obtained from PCA and the reference particle velocities of each area was built by GPR models with the exponential kernel function. Then the trained models are used to determine the cross-sectional velocity distribution only from the particle velocities measured by the non-restrictive electrostatic sensor and the air velocity.

Fig. 10 shows the predicted particle velocities and reference particle velocities of the test dataset in 9 areas under 16 experimental conditions. The predicted velocity values are very close to reference values in all areas. As can be seen from Fig. 9, the distribution of particle velocity on the cross-section of the pipeline is uneven under different experimental conditions. In most cases, the velocity of particles in the central area (A5) of the pipeline is the highest, and the particles in the adjacent areas (A2, A4, A6, A8) travel faster than those in the four corner areas (A1, A3 A7 A9) of the pipeline. Such a phenomenon is due to the influence of the shape of the square-shaped pipe, which hinders the particles from flowing near the four right corners. The particle velocity in the outer side area (A3, A6, A9) of the pipe cross-section is higher than that in the inner area (A1, A5, A7), because the fluid is deflected to the outer side of the pipe due to the influence of centrifugal force at the upstream and downstream bends. The dynamic characteristics of the particles in the measurement section are affected, thus the velocity distribution of particles in the inner areas (A1, A4, A7) changes significantly compared with those in the center and outer areas of the pipeline, which may cause larger prediction errors.

The relative errors between predicted values and the reference values are depicted in Fig. 11. Under all experimental conditions, the relative errors of the predicted velocities in A1 to A9 are all within ±3%. The results suggest that the GPR model is capable of predicting the cross-sectional velocity distribution of particles in a square-shaped pipe based on particle velocities measured by electrostatic sensors along with the velocity of conveying air.

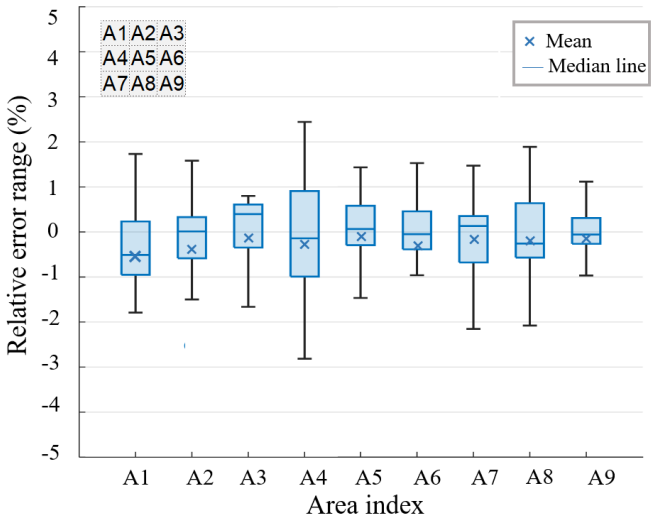

Fig. 11. Relative error range of the predicted velocities in nine areas under all experimental conditions.

TABLE III
TEST SETUP OF SMALLER TRAINING DATASET

Test group	Test dataset not included in the training dataset
Test I	V1M4, V4M1
Test II	V3M1, V3M2, V3M3, V3M4
Test III	V1M3, V2M3 V3M3 V4M3

E. Velocity Prediction Test of Training Dataset under Insufficient Experimental Conditions

Generally, the more comprehensive the data set, the more accurate the model prediction results. However, it is impractical to obtain the training data under all flow conditions in industrial applications. In order to evaluate the performance of the GPR model with a smaller training dataset or missing data, three GPR models that trained using different training datasets were tested with the test datasets shown in Table III, respectively.

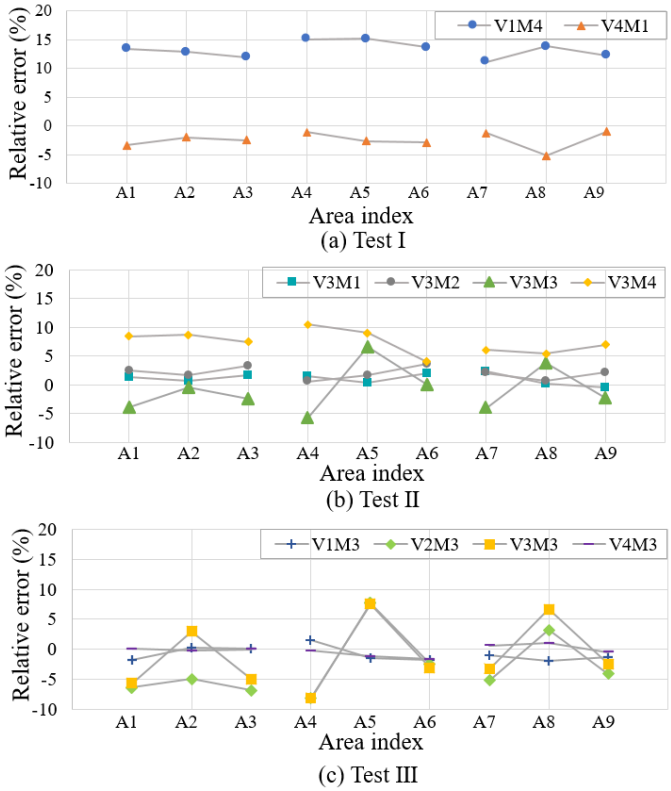

Fig. 12. Relative error for the predicted velocities under different flow conditions.

It is worth noting that the dataset used for training GPR models excludes the flow conditions for testing. In Test I, the GPR model was trained with data from all experimental conditions except for V1M4 (lowest air velocity 19 m/s and highest solid mass flow rate 8 kg/h) and V4M1 (highest air velocity 31 m/s and lowest solid mass flow rate 2 kg/h). The experimental results of these two flow conditions were used to evaluate the trained model. As shown in Fig. 12(a), the relative error of predicted velocity has negative values under the condition of high air velocity and low solid mass flow rate, while the relative error is positive under the condition of low air velocity and high solid mass flow rate. The relative error in all areas is still less than ±5% under the condition of V4M1. However, the relative error of the predicted velocity goes up to the range between 11.60% and 15.16% under the condition of V1M4 because the flow condition is far beyond the training conditions of the model.

In Test II, the training dataset does not contain the data measured at the air velocity of 27 m/s. The developed GPR model was tested under the condition of V3M1, V3M2, V3M3 and V3M4. Fig. 12(b) shows that the relative errors are mostly within ±5% when the solid mass flow rate changes from 2 kg/h to 6 kg/h. When the solid mass flow rate reaches 8 kg/h, larger errors (around 10%) occur in areas A4 and A5. However, compared with the results from Test I, the overall performance is still better than that under the V1M4 flow condition. This is because the test dataset in Test II is unknown to the model but is still within the range of the training dataset.

In Test III, the measurement results under the solid mass flow rate of 6 kg/h were used as the test dataset (not included in the training dataset). The performance of the GPR model under the

conditions of V1M3, V2M3, V3M3 and V4M3 is shown in Fig. 12(c). When the air velocity is 19 m/s and 31 m/s, the relative errors in all areas are less than ±3%. But larger errors (around ±8%) occur in areas A4 and A5 when the air velocity is at 23 m/s and 27 m/s. Due to the uneven distribution of data in the training dataset, these flow conditions were mismatched by the model to other flow conditions, which resulted in larger errors. The result also indicates that more input variables related to flow conditions need to be considered for model training in the follow-up study.

F. Velocity Prediction with Fewer Measurement Electrodes

Measurement instruments with simple structures and low costs are desired in industrial applications as long as their performance meets the requirement. The reduction in the number of electrodes used for measurements can improve the robustness of the system and reduce the costs of hardware. For the modeling process, fewer input variables can accelerate the model training and realize faster prediction. To test the performance of the proposed method with fewer input particle velocities, the model training process was performed by using only the particle velocities measured by the electrode pairs (B, E, H, K) at the center of the four walls of the pipe (as shown in Fig. 2) and the air velocity as input variables. The selected four pairs of electrodes are geometrically symmetrical in the cross-section of the pipeline. Moreover, its installation position is the same as the distance between two adjacent edges, and the measurement sensitivity area formed by these four pairs of electrodes is also symmetrical.

The GPR models were retrained and tested for the particle velocity in 9 areas of the pipe cross-section under 16 environment conditions shown in Table I. The relative error between the predicted result of the models and the reference particle velocities in the testing set is shown in Fig. 13. As can be seen from Fig. 13, the accuracy of the GPR model in each area decreases after the reduction of input variables compared to the results in section D (Fig. 11), and the relative error of particle velocity in area A4 is close to ±5%, while the relative error in the predicted particle velocities for most areas increased by approximately 0.5% compared to the results shown in Fig. 11, except for some areas have smaller values below±3%. Table IV shows the comparison of the training time and prediction time of the GPR models trained using a different number of input velocities. It is obvious that the training speed and prediction speed of the models are improved when the groups of datasets are the same but the number of input variables in each dataset is reduced. In particular, the speed of prediction has been increased by more than three times. In summary, the reduction in input variables made the data sets less abundant, and thus had a slight negative impact on the prediction results.

TABLE IV
COMPARISON OF TRAINING TIME AND PREDICTION SPEED WITH DIFFERENT NUMBER OF INPUT VARIABLES

Number of input variables	Training time (s)	Prediction speed (obs/sec)
13	47	9900
5	41	33000

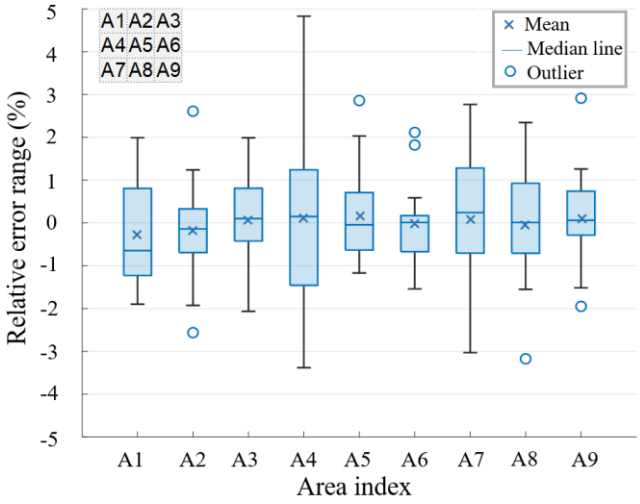

Fig. 13. Relative error range of the predicted velocities in nine areas under all experimental conditions (with fewer measurement electrodes).

V. CONCLUSION

A novel approach using a non-restrictive electrostatic sensor and a GPR model for the measurement of the cross-sectional velocity distribution of pneumatically conveyed particles was proposed and evaluated. The feasibility of the proposed measurement methodology has been verified under laboratory conditions. Experimental results have demonstrated that the GPR model with exponential kernel function trained with the data from all experimental conditions performs well. Compared with other machine learning models, the performance of the GPR model has been verified that GPR has the minimum prediction error (the minimum value of RMSE) and the best fitting effect (the maximum value of R^2). The relative error of predicted velocities in each area using the GPR models is within 3%. With a smaller training dataset, the model performance is negatively affected. For the data beyond the range of the training dataset, the relative error of the model goes up to ±10% or even ±15%. However, the limitation in generalization ability is a common problem for all data-driven models. Therefore, as much data as possible under different flow conditions should be collected when training the model. With fewer measurement electrodes (input variables), the relative error of predicted velocities in each area increases slightly, but remains within 5%. Nevertheless, the model's prediction speed has been increased from 9900 obs/s to 33000 obs/s. In future, validation experiments of the approach will be carried out on larger diameter pipes and field trials will be carried out to assess the methodology under industrial conditions.

REFERENCES

[1] B. Jurjevčič, A. Senegačnik, B. Drobnič, and I. Kuštrin, "The Characterization of Pulverized-Coal Pneumatic Transport Using an Array of Intrusive Electrostatic Sensors," *IEEE Trans. Instrum. Meas.*, vol. 64, no. 12, pp. 3434–3443, Aug. 2015.

[2] X. Qian, Y. Yan, S. Wu, and S. Zhang, "Measurement of velocity and concentration profiles of pneumatically conveyed particles in a square-shaped pipe using electrostatic sensor arrays," *Powder Technol.*, vol. 377, pp. 693–708, Jan. 2021.

[3] Y. Yan, "Mass flow measurement of bulk solids in pneumatic pipelines," *Meas. Sci. Technol.*, vol. 7, no. 12, pp. 1687–1706, Sep. 1996.

[4] Y. Zheng and Q. Liu, "Review of techniques for the mass flow rate measurement of pneumatically conveyed solids," *Measurement*, vol. 44, no. 4, pp. 589–604, May 2011.

[5] N. Furuichi, " Fundamental uncertainty analysis of flowrate measurement using the ultrasonic Doppler velocity profile method," *Flow Meas Instrum.*, vol. 33, pp. 202–211, Oct. 2013.

[6] G. Dinardo, L. Fabbiano, and G. Vacca, "How to directly measure the mean flow velocity in square cross-section pipes," *Flow Meas Instrum.*, vol. 49, pp. 1–7, Jun. 2016.

[7] Y. Yan, Y. Hu, L. Wang, X. Qian, W. Zhang, K. Reda, J. Wu, and G. Zheng, "Electrostatic sensors–Their principles and applications," *Measurement*, vol. 169, Feb. 2021, Art. no. 108506.

[8] Y. Yan, L. Wang, T. Wang, X. Wang, Y. Hu, and Q. Duan, "Application of soft computing techniques to multiphase flow measurement: A review," *Flow Meas. Instrum.*, vol. 60, pp. 30–43, Apr. 2018.

[9] Z. Yang, H. Ji, Z. Huang, B. Wang, and H. Li, "Application of convolution neural network to flow pattern identification of gas-liquid two-phase flow in small-size pipe," *Chinese Automation Congress (CAC)*, Jinan, China, pp. 1389–1393, Oct. 2017.

[10] Z. Xu, F. Wu, L. Zhu, and Y. Li, "LSTM model based on multi-feature extractor to detect flow pattern change characteristics and parameter measurement," *IEEE Sens. J.*, vol. 21, no. 3, pp. 3713–3721, Sep. 2020.

[11] Z. Gao, Z. Qu, Q. Cai, L. Hou, M. Liu and T. Yuan, "A deep branch-aggregation network for recognition of gas–liquid two-phase flow structure," *IEEE Trans. Instrum. Meas.*, vol. 70, pp. 1–8, Sep. 2020.

[12] F. Abbas, L.Wang, Y. Yan, "Mass flow rate measurement of solids in a pneumatic conveying pipeline in different orientations," *Measurement: Sensors*, vol. 10, Nov. 2020, Art. no. 100021.

[13] L. Wang, J. Liu, Y. Yan, X. Wang, and T. Wang, "Gas-liquid two-phase flow measurement using Coriolis flowmeters incorporating artificial neural network, support vector machine, and genetic programming algorithms," *IEEE Trans. Instrum. Meas.*, vol. 66, no. 5, pp. 852–868, Dec. 2016.

[14] H. Wang, M. Zhang, and Y. Yang, "Machine learning for multiphase flowrate estimation with time series sensing data," *Measurement: Sensors*, vol. 10, Nov. 2020, Art. no. 100025.

[15] K. T. Aminu, D. McGlinchey, and A. Cowell, "Acoustic signal processing with robust machine learning algorithm for improved monitoring of particulate solid materials in a gas flowline," *Flow Meas. Instrum.*, vol. 65, pp. 33–44, Mar. 2019.

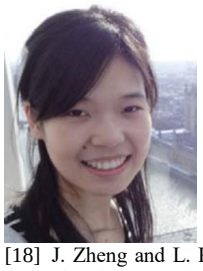

[16] P. Zhang, Y. Yang, Z. Huang, J. Sun, Z. Liao, J. Wang, and Y. Yang, "Machine learning assisted measurement of solid mass flow rate in horizontal pneumatic conveying by acoustic emission detection," *Chem. Eng. Sci.*, vol. 229, Jan. 2021, Art. no. 116083

[17] C. Tan, S. Lv, F. Dong, and M. Takei, "Image reconstruction based on convolutional neural network for electrical resistance tomography" *IEEE Sens. J.*, vol. 19, no. 1, pp. 196–204, Oct. 2018.

[18] J. Zheng and L. Peng, "An autoencoder-based image reconstruction for electrical capacitance tomography," *IEEE Sens. J.*, vol. 18, no. 13, pp. 5464–5474, May 2018.

[19] Y. Yan, L. Xu, and P. Lee, " Mass flow measurement of fine particles in a pneumatic suspension using electrostatic sensing and neural network techniques," *IEEE Trans. Instrum. Meas*, vol. 55, no. 6, pp. 2330–2334, Nov. 2006.

[20] F Abbas, Y. Yan, and L. Wang, "Mass Flow Rate Measurement of Pneumatically Conveyed Solids Through Multimodal Sensing and Data-Driven Modeling," *IEEE Trans. Instrum. Meas*., vol. 70, Aug. 2021, Art. no. 2513416.

[21] J. Li, Y. Qu, C. Li, Y. Xie, Y. Wu, and J. Fan, "Learning local Gaussian process regression for image super-resolution," *Neurocomputing*, vol. 154, pp. 284–295, Apr. 2015.

[22] J. Hu, and J. Wang, "Short-term wind speed prediction using empirical wavelet transform and Gaussian process regression," *Energy*, vol. 93, pp. 1456–1466, Dec. 2015.

[23] Y. Wang, L. Wang, X. Qian, and Y. Yan, "Measurement of cross-sectional velocity distribution of pneumatically conveyed particles in a square-shaped pipe through electrostatic sensing and Gaussian process regression," *Proc. IEEE Int. Instrum. Meas. Technol. Conf. (I2MTC)*, Ottawa, Canada, May 2022, Art. no. 1570781009.

[24] T. Hofmann, B. Schölkopf, A. J. Smola, "Kernel methods in machine learning," *Ann. Stat.*, vol. 36, no. 3, pp. 1171–1220, Feb. 2008.

[25] M. Seeger, "Gaussian processes for machine learning," *Int. J. Neural Syst.*, vol. 14, no. 02, pp. 69–106, Feb. 2004.

[26] M. A. Gelbart, J. Snoek, and R. P. Adams, "Bayesian optimization with unknown constraints," 2014, *arXiv:1403.5607*.

[27] Y. Hu, Y. Yan, X. Qian, and W. Zhang, "A comparative study of induced and transferred charges for mass flow rate measurement of pneumatically conveyed particles," *Powder Technol.*, vol. 356, pp. 715–725, Nov. 2019.

[28] S. Zhang, Y. Yan, X. Qian, and Y. Hu, "Mathematical modeling and experimental evaluation of electrostatic sensor arrays for the flow measurement of fine particles in a square-shaped pipe," *IEEE Sens. J.*, 2016, vol. 16, no. 23, pp. 8531–8541, Sep. 2016.

[29] B. Qi, Y. Yan, W. Zhang, and X. Li, "Experimental investigations into bubble characteristics in a fluidized bed through electrostatic imaging," *Flow Meas. Instrum.*, vol. 70, pp. 1–13, Oct. 2020.

Yongyue Wang received the B.Eng. degree in automation from Shandong University of Technology, Zibo, China, in 2020. She is currently pursuing the M.Sc. degree in measurement technology and instrumentation with North China Electric Power University, Beijing, China.

Her current research interests include measurement of multiphase flow and soft computing.

Xiangchen Qian (Senior Member, IEEE) received the B.Eng. degree in automation from Tianjin University of Technology, Tianjin, China, in 2004, the M.Sc. degree in automatic meter and device from Tianjin University, Tianjin, in 2007, and the Ph.D. degree in electronic engineering from the University of Kent, Canterbury, U.K., in 2013.

He is currently an Associate Professor with the School of Control and Computer Engineering, North China Electric Power University, Beijing, China. His current research interests include multiphase flow measurement techniques, development of instrumentation systems, and SOFC monitoring techniques.

Lijuan Wang (Senior Member, IEEE) received the B.Eng. degree in computer science and technology from Qiqihar University, Heilongjiang, China, in 2010, and the Ph.D. degree in measurement and automation from North China Electric Power University, Beijing, China, in 2015, and the Ph.D. degree in electronic engineering from the University of Kent, Canterbury, U.K., in 2017.

She is currently a Lecturer in electronic engineering with the School of Engineering, University of Kent. Her current research interests include electrostatic sensing, multiphase flow measurement, condition monitoring of mechanical systems, sensors and instrumentation systems, data analysis, and soft computing.

Yong Yan (Fellow, IEEE) received the B.Eng. and M.Sc. degrees in instrumentation and control engineering from Tsinghua University, Beijing, China, in 1985 and 1988, respectively, and the Ph.D. degree in flow measurement and instrumentation from the University of Teesside, Middlesbrough, U.K., in 1992.

He was an Assistant Lecturer with Tsinghua University in 1988. In 1989, he joined the University of Teesside as a Research Assistant. After a short period of Post-Doctoral Research, he was a Lecturer with the University of Teesside from 1993 to 1996, and then as a Senior Lecturer, a Reader, and a Professor with the University of Greenwich, Chatham, U.K., from 1996 to 2004. He is currently a Professor of electronic instrumentation and the Director of innovation at the School of Engineering and Digital Arts, the University of Kent, Canterbury, U.K. His current research interests include multiphase flow measurement, combustion instrumentation, intelligent measurement and condition monitoring.

Dr. Yan was elected as a Fellow of the Royal Academy of Engineering in 2020. He was awarded the gold medal in 2020 by the IEEE TRANSACTIONS ON INSTRUMENTATION AND MEASUREMENT as the most published author of all time from the U.K.